Electrically detected HYSCORE on conduction band tail states in ^{29}Si-enriched microcrystalline silicon

Christoph Meier, Christian Teutloff, Robert Bittl, and Jan Behrends

Berlin Joint EPR Lab, Fachbereich Physik,

Freie Universität Berlin, Arnimallee 14, D-14159 Berlin, Germany

Oleksandr Astakhov and Friedhelm Finger

Forschungszentrum Jülich, Institut für Energie- und

Klimaforschung 5 – Photovoltaik, D-52425 Jülich, Germany

(Dated: March 3, 2015)

Abstract

Electrically detected hyperfine sublevel correlation (ED-HYSCORE) measurements are presented and employed to study spin-dependent transport in thin-film microcrystalline silicon solar cells. We explore the hyperfine coupling between paramagnetic conduction band tail states involved in hopping transport and neighboring ^{29}Si nuclei at low temperature ($T = 5$ K). ED-HYSCORE measurements performed on solar cells with ^{29}Si-enriched absorber layers reveal that the hyperfine interaction between these current-influencing centers and ^{29}Si nuclei in the surroundings is dominated by isotropic couplings up to ~ 4 MHz, whereas the anisotropic contributions are small. This indicates that the wave function of the conduction band tail states is distributed over several nuclei. Our results demonstrate that the ED-HYSCORE technique can provide helpful insight into the microscopic structure of transport-relevant paramagnetic states and thus usefully complements the toolbox of electrically detected magnetic resonance spectroscopy.

I. INTRODUCTION

Transport and recombination processes in semiconductors often involve transitions between localized electronic states. Provided that two adjacent states are each occupied with a single charge carrier, the transfer rate towards the formation of a doubly occupied state will, among other factors, depend on the relative orientation of the spins of both charge carriers forming the pair. If this transfer rate is the limiting step in a recombination or hopping process, the spin state of this *doublet pair* comprising two $S = 1/2$ centers will affect charge transport[1,2]. This has a direct influence on observables such as luminescence or electrical conductivity. Resonant excitation of one or both spins forming a weakly coupled pair induced by microwave (mw) radiation as in conventional electron paramagnetic resonance (EPR) spectroscopy changes the singlet and triplet content of the pair. This can influence the probability for a recombination or hopping process and thus results in changes of macroscopic observables. Monitoring these changes allows analyzing spin-dependent processes and the structure of the contributing paramagnetic centers with a detection sensitivity that is substantially higher than in classical EPR spectroscopy[3–5].

Transport and recombination processes of excess charge carriers are critical for the performance of solar cells. In particular thin-film silicon solar cells with disordered amorphous or microcrystalline hydrogenated silicon (a-Si:H and μc-Si:H) absorbers possess a variety of trapping and recombination states in the band gap[6,7]. In μc-Si:H for instance conduction band tail states (referred to as CE states because they were originally assigned to conduction electrons)[8,9] and dangling bonds (db states)[9,10] are the most prominent examples.

Electrically detected magnetic resonance (EDMR) spectroscopy is well-suited to study these processes via localized states. First applied to thin-film silicon[11], most studies were based on continuous wave EDMR experiments in which the sample is continuously subjected to mw radiation, and the resonant current change is detected as a function of the magnetic field to yield information on the g-values and spectral features of the conductivity-influencing paramagnetic centers. More recently pulsed (p) EDMR using short mw pulses to manipulate spin-dependent transition rates in combination with time-resolved current detection has evolved as a valuable tool to elucidate the dynamics of spin-dependent processes[12]. Further, the development of pEDMR has paved the way for transferring many advanced EPR techniques to the EDMR world[13,14]. Especially EPR experiments that explore the microscopic

environment of a paramagnetic center by probing the hyperfine (HF) interaction between the electron spin and nuclear spins in its vicinity were recently modified such that they are compatible with an electrical detection scheme. Electrically detected electron spin echo envelope modulation (ED-ESEEM) measurements were employed to elucidate the interaction between paramagnetic sites and nuclear spins in solar cells based on a-Si:H and μc-Si:H[15] and at the interface between crystalline silicon (c-Si) and silicon dioxide[16]. Electrically detected electron nuclear double resonance (ED-ENDOR) spectroscopy was demonstrated on phosphorus donors in c-Si[17,18].

ED-ENDOR experiments are well-suited for studying nuclei that exhibit strong HF couplings. This applies to e.g. ^{31}P in c-Si where the intense narrow ENDOR lines are centered around $\sim$ 58 MHz for X-band mw frequencies. The radio frequency (RF) pulses used for manipulating the nuclear spins inevitably cause strong interference signals in the current detection circuit, which, in the case of ^{31}P in c-Si, can conveniently be removed by inserting a bandpass filter. For nuclei with (1) small nuclear g-factor, (2) weak HF couplings and (3) broader HF distributions as for ^{29}Si or protons in disordered a-Si:H and μc-Si:H the situation is less favorable. In this case RF signal filtering would result in a substantial deterioration of the pEDMR transient signal typically exhibiting time constants in the low microsecond regime. Using higher mw resonance frequencies can help to circumvent this problem, but is accompanied with other technical difficulties[19]. In contrast, ED-ESEEM measurements require less technical efforts and are particularly sensitive to small HF couplings. ED-ESEEM was shown to provide structural information on current-influencing paramagnetic states in disordered as well as in crystalline silicon[15,16].

The introduction of the hyperfine sublevel correlation (HYSCORE) technique has led to a significant resolution enhancement in mw-detected ESEEM spectroscopy[20,21]. Following these lines, we demonstrate the feasibilty of HYSCORE measurements in combination with electrical detection. We utilize the advantages of HYSCORE as compared to one-dimensional ESEEM experiments known from conventional EPR spectroscopy and report ED-HYSCORE measurements performed on thin-film solar cells with ^{29}Si-enriched μc-Si:H absorber layers at low temperature. The hyperfine interaction between current-influencing conduction band tail states and neighboring ^{29}Si nuclei is shown to be dominated by comparatively small isotropic couplings with many nuclei for each paramagnetic center. This indicates a rather delocalized nature of the conduction band tail states contributing to spin-dependent hopping

transport in μc-Si:H.

II. MATERIALS AND METHODS

A. Samples

In this EDMR study μc-Si:H thin-film solar cells produced in a p-i-n layer configuration were employed. Doped and intrinsic thin-film silicon layers were prepared by plasma enhanced chemical vapor deposition (PECVD) using optimized standard deposition conditions[22]. The sample consisted of a stack with 800 nm texture-etched ZnO, boron-doped p-μc-Si:H, ≈ 1 μm intrinsic μc-Si:H absorber, phosphorus-doped n-μc-Si:H and ZnO with silver as a back contact. For the investigation of the ^{29}Si hyperfine interaction in μc-Si:H the silicon isotope composition of the intrinsic layer was varied.

On the one side, silane gas with ≈ 50% $^{29}SiH_4$ concentration was used (yielding the ^{29}Si-sample) to deposit an intrinsic μc-Si:H layer rich of magnetic ^{29}Si nuclei. On the other side, the ^{28}Si-sample with an intrinsic layer free of spin-carrying ^{29}Si was produced as a reference with the help of $^{28}SiH_4$-enriched silane gas (concentration > 99.9%).

The silane concentration of $SC = 4\%$ in the deposition gas mixture led to an intrinsic μc-Si:H crystalline volume fraction of $I_c = 67\%$ and 74% for the ^{29}Si- and ^{28}Si-sample, respectively. Due to technical reasons the thin n- and p-doped layers (≈ 30 nm thickness) of both cells were produced using silane of natural Si isotope composition (^{29}Si concentration 4.7%).

B. Experimental conditions

All EDMR measurements were carried out on a BRUKER E580 spectrometer with a dielectric ring resonator (EN4118X-MD4) working at microwave frequencies of 9.7 GHz (≈ 350 mT). The sample cooling was realized by a Helium flow cryostat and a temperature controller ITC503 from Oxford Instruments to perform experiments at $T = 5$ K (80 K). Short pulses of down to $t_\pi = 20$ ns for a π-pulse were available for the pEDMR experiments due to a 1 kW traveling wave tube mw amplifier.

A combined voltage source and current amplifier (Elektronik Manufaktur Mahlsdorf) was used to detect the photocurrent and EDMR signal[23]. The solar cell was operated in reverse

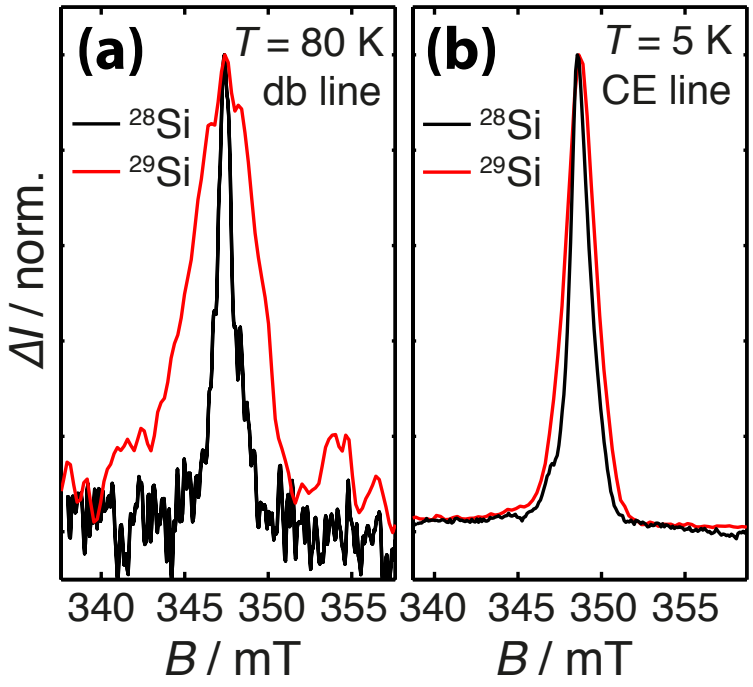

FIG. 1. Normalized field-swept spectra of the ^{28}Si- and ^{29}Si-samples. a) At 80 K the single db signal ($g_{\mathrm{db}} = 2.0046(3)$) is observed. b) At 5 K the spectrum shows mainly the CE signal ($g_{\mathrm{CE}} = 1.9978(3)$). The width of the CE line increases from $\Delta B^{28}_{\mathrm{CE}} = 1.5(1)$ mT to $\Delta B^{29}_{\mathrm{CE}} = 2.2(1)$ mT, whereas the db line width grows by a factor of ≈ 5 to $\Delta B^{29}_{\mathrm{db}} = 4.8(2)$ mT (the data points at 80 K were slightly smoothed for clarity).

bias direction ($U = -1$ V). Under illumination (halogen cold light source, $P = 150$ W) through the optical window in the resonator a photocurrent of $I_{\mathrm{ph}} \approx 16$ µA ($I_{\mathrm{ph}} = 41 - 126$ µA) was measured at $T = 5$ K ($T = 80$ K).

III. RESULTS AND DISCUSSION

In a first step, µc-Si:H db and CE signals which were measured at different temperatures in the EDMR spectra of the ^{29}Si- and ^{28}Si-sample are evaluated with respect to their dependence on the ^{29}Si HF interaction. Fig. 1 shows the field-swept pEDMR spectra of both samples at $T = 5$ K and 80 K. They were recorded as a transient current change after a 300 ns π-pulse (see the scheme in Fig. 2 (a)). The long π-pulse was chosen to avoid line broadening caused by the pulse band width.

At 80 K (Fig. 1 (a)) an EDMR signal due to dangling bond defects is observed at

$g_{\mathrm{db}} = 2.0046(3)$[23,24]. The resonant current change is negative with respect to the photocurrent (*quenching signal*), which indicates that this defect takes part in charge carrier recombination in the microcrystalline material[23,25]. The line width of the signal increases significantly upon ^{29}Si enrichment from $\Delta B_{\mathrm{db}}^{28} = 1.0(1)$ mT to $\Delta B_{\mathrm{db}}^{29} = 4.8(2)$ mT. This additional broadening is caused by HF coupling between electron spins and ^{29}Si nuclei in the environment. A wide distribution of coupling constants results in a featureless broad line. This observation is consistent with findings in hyperfine studies of dangling bonds in amorphous silicon[26]. Studies for db defects in microcrystalline silicon are, to our knowledge, not available. Biegelsen and Stutzmann found an overall broadening of the a-Si:H dangling bond spectrum, when they increased the ^{29}Si content from 4.7% to 93%. Furthermore, they detected a large HF splitting of ≈ 7 mT (200 MHz), which separates the db resonance into a doublet structure. This large coupling is not found in our spectra, since a complete splitting is only observable when all silicon nuclei are substituted to ^{29}Si. For the 50% enrichment in our samples a central line that is not affected by this large HF interaction overlaps with HF satellites resulting in a broad single line. From this strong HF broadening with a considerable fraction of coupling constants above ≈ 3 mT (90 MHz) we can conclude that the dangling bond defect in μc-Si:H can be seen as a rather localized defect comparable to its counterpart in a-Si:H.

At 5 K (Fig. 1 (b)) the EDMR spectrum is dominated by a signal at $g_{\mathrm{CE}} = 1.9978(3)$. It is attributed to hopping transport via CE states in the crystalline parts of the microcrystalline material[15,23]. Signals due to dangling bond defects and holes in the material contribute with only smaller intensity. In addition, it is possible to obtain spectra with an isolated CE line utilizing deconvolution methods based on the dynamics of the transient EDMR signals[19,27]. Comparing the CE spectra of ^{29}Si- and ^{28}Si-sample reveals that the HF broadening by ^{29}Si nuclei is much less pronounced. The line width increases by less then 1 mT and HF satellites are not resolved. This indicates that the identity of the CE center in microcrystalline silicon is markedly different from that of the localized db defect.

Precise conclusions about the hyperfine structure of dangling bonds and CE centers in ^{29}Si-enriched microcrystalline silicon solely from field-swept spectra cannot be drawn, since the HF signatures of both paramagnetic centers emerge as an unresolved broadening. Hence, it is necessary to employ methods, which allow direct access to nuclear frequencies.

Thus, we will employ electrically detected 2-pulse ESEEM (2pESEEM) and 3-pulse ES-

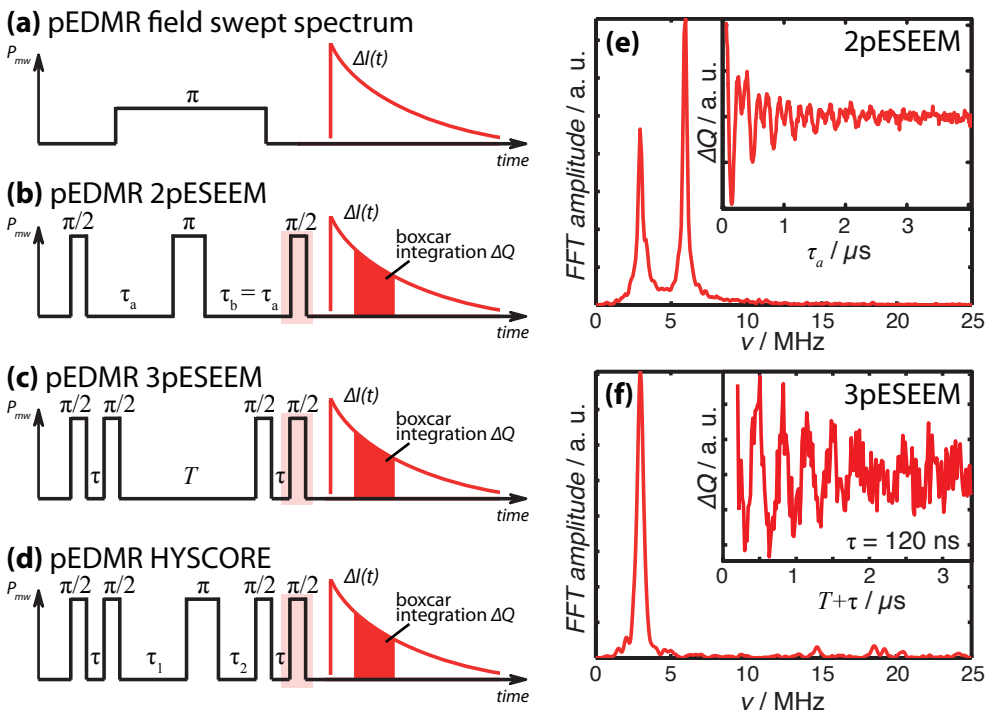

FIG. 2. (a) - (d) Overview of the applied pulse sequences. (a) A single π-pulse is used for field-swept experiments. The resonant current response $\Delta I(t)$ is detected after the pulse. (b) For electrically detected 2pESEEM the standard spin echo pulse sequence is augmented by a $\pi/2$ readout pulse (shaded red). (c) The stimulated echo pulse sequence together with the $\pi/2$ readout pulse for EDMR is employed for 3pESEEM. (d) The standard EPR HYSCORE sequence complemented by the readout pulse is used for ED-HYSCORE. (e) Frequency spectrum of the 2pESEEM experiment on the CE resonance position. The inset shows the time domain signal without the unmodulated background. (f) Frequency spectrum of the 3pESEEM experiment. In the inset the modulating part of the time domain signal is given.

EEM (3pESEEM) as well as HYSCORE experiments to study the ^{29}Si HF structure of the μc-Si:H CE center. Due to the low EDMR signal quality these methods could not be applied to the db resonance.

A. Electrically detected electron spin echo envelope modulation (ED-ESEEM)

The CE signal is due to a spin-dependent hopping transport process involving weakly coupled electron spins $S = 1/2$ in neighboring CE states[28,29]. These electron spins inter-

act with nearby ^{29}Si nuclear spins $I = 1/2$. For the following evaluation of ESEEM and HYSCORE data this quite complicated spin system can be treated as a system consisting of a single spin $S = 1/2$ coupled to a nuclear spin $I = 1/2$ provided that selective excitation of only one electron spin is present[15,30]. This allows us to make use of the theoretical concepts of the $(S = 1/2, I = 1/2)$ model system.

An ESEEM effect is observed when S and I are coupled via an anisotropic HF interaction. Under these conditions otherwise forbidden transitions with ($\Delta m_S = \pm 1$, $\Delta m_I = \pm 1$) become weakly allowed, so that the echo amplitude in spin echo experiments is modulated by nuclear frequencies $\omega_{\alpha/\beta} = \sqrt{(\frac{1}{2}a \pm \omega_\mathrm{I})^2 + \frac{1}{4}b^2}$, where ω_I is the nuclear Larmor frequency and a, b are the secular and pseudo-secular part of the HF interaction which are given by $a = A_\mathrm{iso} + A_\mathrm{dip}(3\cos^2\theta - 1)$ and $b = 3A_\mathrm{dip}\sin\theta\cos\theta$[21]. A_iso and A_dip are the isotropic and anisotropic HF interaction and θ describes the angle between external magnetic field vector and the axis connecting the electron and nuclear spins. The modulation depth parameter $K = (\frac{b\omega_\mathrm{I}}{\omega_\alpha\omega_\beta})^2$ is maximum between ω_I and $2\omega_\mathrm{I}$, which restricts ESEEM experiments to studies of HF couplings in the range of the nuclear Larmor frequency.

The 2pESEEM experiment based on the two-pulse echo sequence $\pi/2{-}\tau_a{-}\pi{-}\tau_b{-}$echo has already been adapted for electrical detection[15,16]. In this experiment the electron coherences excited by the first pulse are refocussed at time $\tau_b = \tau_a$ to build up a spin echo whose modulating amplitude is detected in dependence on τ_a (Fig. 2 (b)). The 2pESEEM frequency spectrum shows signals at ω_α and ω_β as well as their sum and difference frequencies $\omega_\pm = \omega_\alpha \pm \omega_\beta$. This often results in complicated spectra due to overlapping lines (see e.g. Ref.[15]).

In 3pESEEM an echo envelope modulation is observed when the time delay T between the second and the third pulse of the stimulated echo sequence ($\pi/2{-}\tau{-}\pi/2{-}T{-}\pi/2{-}\tau{-}$echo) is incremented (Fig. 2 (c)). The echo amplitude is measured as function of $T + \tau$, which reveals the fundamental oscillation frequencies ω_α and ω_β. This significantly simplifies the frequency spectra. In addition, the spectral resolution is increased compared to 2pESEEM, because the ESEEM traces and with this the line widths in the frequency spectra are not limited by the electron spin phase memory time T_M as in 2pESEEM, but by the spin-lattice relaxation time T_1, which is much longer. Disadvantageous is, that modulation depths are relatively small and so-called blind spots appear in the ESEEM spectrum whenever $\omega_{\alpha/\beta} \cdot \tau$ is a multiple of 2π[21].

For the adaptation to EDMR the ESEEM pulse sequences are augmented by a $\pi/2$ read-

out pulse at the time of echo formation to transfer the electron coherences to polarizations[31]. To remove mw background signals from the 2pESEEM trace a 2-step phase cycling is applied[32]. In 3pESEEM measurements the 8-step standard phase cycling filters mw background as well as unwanted echo signals interfering with the detected stimulated echo[21]. Finally, boxcar integration of the current response $\Delta I(t)$ yields the ESEEM signal ΔQ, which is proportional to the echo amplitude.

In Fig. 2 (e) and (f) the results of the 2p- and 3pESEEM measurements on the CE resonance position are shown. For both experiments short pulses ($t_{\pi/2} = 10$ ns and $t_\pi = 20$ ns) were used to measure ≈ 4 µs and ≈ 3.4 µs long time traces. The initial inter-pulse delays could be chosen as short as $\tau_a = 60$ ns and $T = 100$ ns, since electrical detection is not affected by resonator dead time effects. $\Delta I(t)$ was integrated between 2 and 6 µs. The obtained signal decay was biexponentially fitted and the fit was subtracted to remove the unmodulated part. The remaining modulated part is used to obtain the ESEEM frequency spectra by fast-Fourier transformation (FFT).

The ESEEM spectra can be fully described by assuming that only ^{29}Si nuclei with $\nu_\mathrm{I} = 2.96$ MHz at $B = 349.2$ mT couple to the electron spins. All signals have a line width of $\Delta\nu < 0.5$ MHz corresponding to the decay of ESEEM modulation. However, it is remarkable that the width of the line centered near ν_I is the same as for the typically narrow feature at $\nu_+ \approx 2\nu_\mathrm{I}$ in the 2pESEEM spectrum. As shown above, $\nu_{\alpha/\beta}$ depends on the HF parameters a and b. When considerable HF interaction is present, ν_α and ν_β are split symmetrically around ν_I. In case of a distribution of HF couplings the line pairs add up to a broad signal of reduced intensity. This is not observed here, which means that the HF structure of the CE centers is dominated by small couplings. For a more detailed investigation of this HF structure, we applied electrically detected HYSCORE to the sample. Compared with ESEEM methods HYSCORE has two main advantages in the present case. First, it is possible to discriminate between spectral contributions from weakly and strongly coupled nuclei which may overlap in ESEEM spectra and, second, estimations of A_iso and A_dip can be achieved.

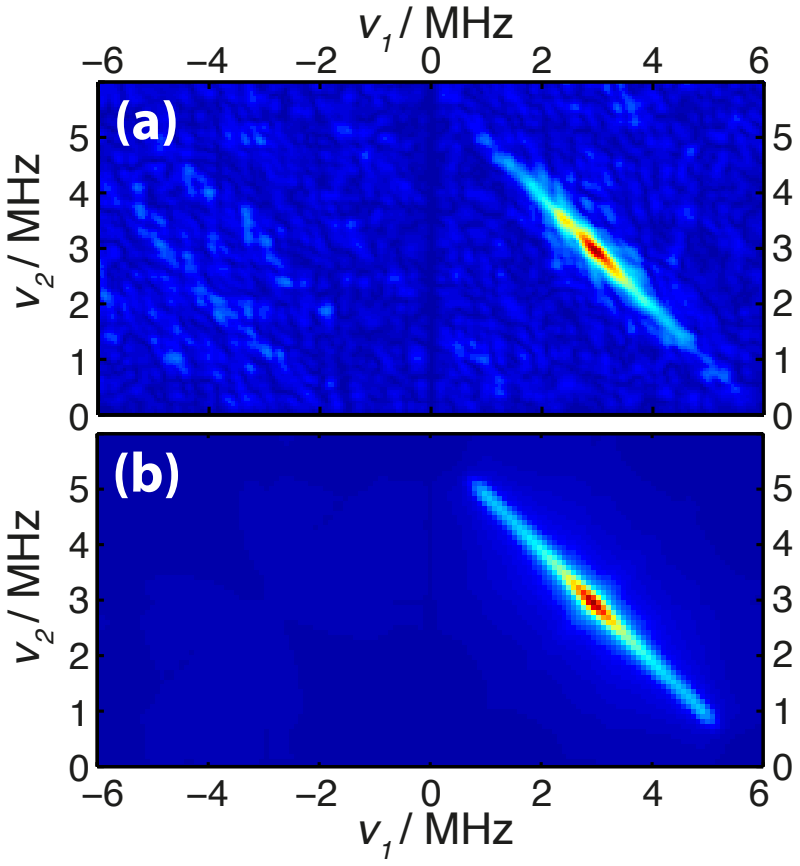

FIG. 3. Experimental and simulated ED-HYSCORE data measured on the CE resonance position. (a) First and second quadrant of the experimental frequency-domain spectrum. (b) Simulated frequency spectrum. Detailed information is given in the text.

B. Electrically detected hyperfine sublevel correlation (ED-HYSCORE)

The four-pulse sequence $\pi/2-\tau-\pi/2-\tau_1-\pi-\tau_2-\pi/2-\tau-$echo is used for HYSCORE as shown in Fig. 2 (d)[21,33]. In this experiment the echo amplitude is detected as a function of the independently incremented times τ_1 and τ_2. The time domain signal shows up as echo-shaped modulation of the electron spin echo at about $\tau_2 = \tau_1$. After FFT along both dimensions a 2D map of the hyperfine structure is obtained. In the case of weak coupling ($2|\omega_\mathrm{I}| > |A_\mathrm{iso}|$) a pair of correlation peaks appears at $(\omega_\alpha, \omega_\beta)$ and $(\omega_\beta, \omega_\alpha)$, which is well separated from the pair of cross-peaks at $(\omega_\alpha, -\omega_\beta)$ and $(\omega_\beta, -\omega_\alpha)$ found in the strong coupling case ($2|\omega_\mathrm{I}| < |A_\mathrm{iso}|$). We note that every peak (ω_1, ω_2) is accompanied by a twin peak at $(-\omega_1, -\omega_2)$, so that two adjacent quadrants in the 2D spectrum contain the complete spectral information. Further details about HYSCORE can be found in the

literature[20,21,33,34].

The four-pulse sequence is expanded by an additional $\pi/2$-pulse at the time of echo formation for the electrical detection. A 16-step phase cycling conventionally used in EPR is employed to get rid of unwanted background signals and echoes[21]. The resulting current response $\Delta I(t)$ is integrated between 2 and 6 µs yielding the final signal ΔQ. The pulse lengths were chosen as in the ESEEM experiments, τ was set to 150 ns to avoid blind spots in the obtained frequency range. The total accumulation time for the data set with ≈ 7µs long τ_1- and τ_2-traces was nearly 12 hours. Finally, the time traces were translated to frequency spectra by FFT.

In Fig. 3 (a) the frequency map of the ED-HYSCORE experiment is shown. All contributions to the spectrum are found in the first quadrant, which means that ^{29}Si nuclei are weakly coupled to the electron spin. Additional measurements with a larger frequency range of ± 8 MHz did not reveal signals in the strong coupling quadrant. We recognize a ridge centered around the silicon Larmor frequency. An estimate of the maximum hyperfine coupling of $A_{\mathrm{max}} \approx 4$ MHz to the ^{29}Si nuclei follows from the width of the ridge measured parallel to one of the axes. The ridge does not show any bending which points to a small influence of A_{dip}.

These experimental data are compared to numerical simulations of HYSCORE spectra obtained by the EPR toolbox *easyspin*[35] implemented in MATLAB (The Mathworks, Natick, MA, USA). The simulated HYSCORE spectrum consists of a sum of single spectra based on spin systems ($S = 1/2, I = 1/2$) with individual HF parameters to take the aspect of distributed HF couplings into account. Altogether 14 spectra were simulated and summed up based on isotropic couplings A_{iso} spread between 0.05 MHz and 4 MHz, whereas the anisotropic part A_{dip} was chosen small and kept constant. The final HYSCORE spectrum obtained for $A_{\mathrm{dip}} = 0.3$ MHz is shown in (Fig. 3 (b)). Such spectra were simulated for several values of A_{dip}. The best accordance between experiment and simulation is found for $|A_{\mathrm{dip}}| \leq 0.5$ MHz. Beyond this range A_{dip} leads to a substantial bending of the ridge which is not consistent with our experimental data.

IV. CONCLUSIONS

The results of the EDMR measurements allow us to draw conclusions on the microscopic environment of current-influencing conduction band tail states in μc-Si:H. The CE center HF data observed in the field-swept spectra, ESEEM and HYSCORE can be interpreted as follows: The HYSCORE spectra show a distribution of HF couplings of up to ≈ 4 MHz with ^{29}Si nuclei in the surroundings of the unpaired electrons. The interaction is dominated by isotropic HF coupling, whereas the anisotropic contributions are small. Larger couplings can be excluded based on 2p- and 3pESEEM measurements. These results indicate that the wave function of the CE state is distributed over many ^{29}Si nuclei without having a center of electron density at one nucleus or a few nuclei. Such a delocalized wave function can be explained by the composite structure of μc-Si:H: Microcrystalline silicon is a heterogeneous material with crystalline grains (with diameters of a few nanometers) embedded in a matrix of amorphous silicon. When the crystalline volume fraction is sufficiently large, the crystallites agglomerate in clusters, giving rise to a columnar structure parallel to the μc-Si:H layer growth direction[36,37]. Within this material the CE centers are assigned to the crystalline regions[15], which are depleted from most kinds of lattice defects. Their EPR signal has a g-value at $g_{\mathrm{CE}} \approx 1.997$ resembling that of conduction electrons in c-Si[38] and the EPR signal intensity of the CE state is proportional to the μc-Si:H conductivity[39]. The wave function of the CE center is assumed to be delocalized over many ^{29}Si nuclei in the crystallite, thus causing weak HF interaction. As a result, the dipolar interaction partly averages out, leading to negligibly small values for A_{dip} and a broad distribution for A_{iso}. This gives rise to the rather narrow and unresolved line observed in the ED-HYSCORE spectrum.

The field-swept EDMR spectra exhibit unresolved ^{29}Si HF broadening of the CE signal, which is small compared to the influence of ^{29}Si nuclei on the dangling bond EDMR signal, but much larger than the maximum HF coupling constant found in the HYSCORE spectra. This is consistent with the interpretation that the CE state wave function is substantially more delocalized than the wave function of dangling bond defects in μc-Si:H. Our results are in agreement with the prevailing model assuming that the CE state is a paramagnetic center sharing many similarities with conduction electrons in c-Si with the difference that Si crystallites of finite size accommodate the CE centers.

V. PERSPECTIVES

This study demonstrates that ED-HYSCORE experiments can provide valuable information on conductivity-influencing paramagnetic states in disordered semiconductors. We have chosen ^{29}Si-enriched μc-Si:H as an exemplary material, but the application of ED-HYSCORE is certainly not limited to isotope-enriched materials. There are a number of questions where e.g. the HF interaction between paramagnetic centers and neighboring protons can be utilized to obtain information on charge transport pathways. This is particularly true for disordered organic semiconductors used as absorbers in organic solar cells. Previous studies have shown that conventional HYSCORE measurements are suitable to quantify the HF interaction between charge carriers (polarons) and ^{1}H nuclei and that this information can be used to determine the degree of polaron delocalization in this class of materials[40]. In addition, spin-dependent processes via doublet pairs influence polaron transport in organic semiconductors even at room temperature[41]. This allows for pEDMR studies exploiting coherent spin effects under realistic solar-cell operating conditions[42,43] and hence provides the basis for ED-HYSCORE measurements on organic solar cells. This opens the intriguing perspective to determine the localization of photogenerated polarons, which is considered a key parameter determining the charge carrier mobility[44] and thus critically influences the quantum efficiency of organic solar cells.

ACKNOWLEDGMENTS

We thank K.-P. Dinse for helpful discussions and gratefully acknowledge financial support from BMBF (EPR-Solar network project 03SF0328), DFG (SPP 1601) and the Helmholtz Association (Energie-Allianz Hybrid-Photovoltaik).

---

[1] D. Kaplan, I. Solomon, N.F. Mott, Journ. de Phys. Lettr. **39**(4), L51 (1978)

[2] C. Boehme, K. Lips, in *Charge transport in disordered solids with applications in electronics*, ed. by S. Baranovski (Wiley, Chichester, England; Hoboken, NJ, 2006), pp. 179–219

[3] K.M. Salikhov, Y.N. Molin, R.Z. Sagdeev, *Spin Polarization and Magnetic Effects in Radical Reactions* (Elsevier, 1984)

[4] R.H. Clarke (ed.), *Triplet State ODMR Spectrocopy* (John Wiley & Sons, New York, 1982)

[5] D.R. McCamey, H. Huebl, M.S. Brandt, W.D. Hutchison, J.C. McCallum, R.G. Clark, A.R. Hamilton, Appl. Phys. Lett. **89**(18), 182115 (2006)

[6] R.A. Street, *Hydrogenated amorphous silicon* (Cambridge University Press, 2005)

[7] R.E.I. Schropp, M. Zeman, *Amorphous and Microcrystalline Silicon Solar Cells: Modeling, Materials and Device Technology* (Kluwer, Boston, 1998)

[8] F. Finger, C. Malten, P. Hapke, R. Carius, R. Flückiger, H. Wagner, Philos. Mag. Lett. **70**(4), 247 (1994)

[9] K. Lips, P. Kanschat, W. Fuhs, Solar Energy Materials and Solar Cells **78**(1-4), 513 (2003)

[10] F. Finger, J. Müller, C. Malten, H. Wagner, Philos. Mag. B - Physics of Condensed Matter Statistical Mechanics Electronic Optical and Magnetic Properties **77**(3), 805 (1998)

[11] M. Stutzmann, M.S. Brandt, M.W. Bayerl, J. Non-Cryst. Solids **266-269**, 1 (2000)

[12] C. Boehme, K. Lips, Appl. Phys. Lett. **79**(26), 4363 (2001)

[13] C. Boehme, K. Lips, Phys. Rev. Lett. **91**(24), 246603 (2003)

[14] A. Schnegg, J. Behrends, M. Fehr, K. Lips, Phys. Chem. Chem. Phys. **14**(42), 14418 (2012)

[15] M. Fehr, J. Behrends, S. Haas, B. Rech, K. Lips, A. Schnegg, Phys. Rev. B **84**(19), 193202 (2011)

[16] F. Hoehne, J. Lu, A.R. Stegner, M. Stutzmann, M.S. Brandt, M. Rohrmueller, W.G. Schmidt, U. Gerstmann, Phys. Rev. Lett. **106**(19), 196101 (2011)

[17] D.R. McCamey, J. Van Tol, G.W. Morley, C. Boehme, Science **330**(6011), 1652 (2010)

[18] F. Hoehne, L. Dreher, H. Huebl, M. Stutzmann, M.S. Brandt, Phys. Rev. Lett. **106**, 187601 (2011)

[19] C. Meier, J. Behrends, C. Teutloff, O. Astakhov, A. Schnegg, K. Lips, R. Bittl, J. Magn. Reson. **234**, 1 (2013)

[20] P. Höfer, A. Grupp, H. Nebenführ, M. Mehring, Chem. Phys. Lett. **132**(3), 279 (1986)

[21] A. Schweiger, G. Jeschke, *Principles of Pulse Electron Paramagnetic Resonance* (Oxford University Press, 2001)

[22] W. Böttler, V. Smirnov, J. Hupkes, F. Finger, phys. stat. sol. A - Applications and Materials Science **209**(6), 1144 (2012)

[23] J. Behrends, A. Schnegg, M. Fehr, A. Lambertz, S. Haas, F. Finger, B. Rech, K. Lips, Philos. Mag. **89**(28-30), 2655 (2009)

[24] F. Finger, L.B. Neto, R. Carius, T. Dylla, S. Klein, phys. stat. sol. (c) **1**(5), 1248 (2004)

[25] K. Lips, C. Boehme, W. Fuhs, IEE Proceedings - Circuits Devices and Systems **150**(4), 309 (2003)

[26] D.K. Biegelsen, M. Stutzmann, Phys. Rev. B **33**(5), 3006 (1986)

[27] J. Behrends, A. Schnegg, C. Boehme, S. Haas, H. Stiebig, F. Finger, B. Rech, K. Lips, J. Non-Cryst. Solids **354**(19-25), 2411 (2008)

[28] P. Kanschat, K. Lips, W. Fuhs, J. Non-Cryst. Solids **266**, 524 (2000)

[29] C. Meier, J. Behrends, R. Bittl, Mol. Phys. **111**(18-19), 2683 (2013)

[30] G. Zwanenburg, P.J. Hore, J. Magn. Res. Series A **114**(2), 139 (1995)

[31] H. Huebl, F. Hoehne, B. Grolik, A.R. Stegner, M. Stutzmann, M.S. Brandt, Phys. Rev. Lett. **100**(17), 177602 (2008)

[32] F. Hoehne, L. Dreher, J. Behrends, M. Fehr, H. Huebl, K. Lips, A. Schnegg, M. Suckert, M. Stutzmann, M.S. Brandt, Rev. Sci. Instrum. **83**(4), 043907 (2012)

[33] J. Harmer, G. Mitrikas, A. Schweiger, in *High Resolution EPR*, *Biological Magnetic Resonance*, vol. 28, ed. by G. Hanson, L. Berliner (Springer Science+Business Media, 2009), chap. 2, pp. 13 – 61

[34] A. Ponti, A. Schweiger, J. Chem. Phys. **102**(13), 5207 (1995)

[35] S. Stoll, A. Schweiger, J. Magn. Reson. **178**(1), 42 (2006)

[36] L. Houben, M. Luysberg, P. Hapke, R. Carius, F. Finger, H. Wagner, Philos. Mag. A - Physics of Condensed Matter Structure Defects and Mechanical Properties **77**(6), 1447 (1998)

[37] M. Luysberg, P. Hapke, R. Carius, F. Finger, Philos. Mag. A- Physics of Condensed Matter Structure Defects and Mechanical Properties **75**(1), 31 (1997)

[38] C.F. Young, E.H. Poindexter, G.J. Gerardi, W.L. Warren, D.J. Keeble, Phys. Rev. B **55**(24), 16245 (1997)

[39] F. Finger, J. Müller, C. Malten, R. Carius, H. Wagner, J. Non-Cryst. Solids **266**, 511 (2000)

[40] A. Aguirre, P. Gast, S. Orlinskii, I. Akimoto, E.J.J. Groenen, H.E. Mkami, E. Goovaerts, S.V. Doorslaer, Phys. Chem. Chem. Phys. **10**(47), 7129 (2008)

[41] O. Mermer, G. Veeraraghavan, T.L. Francis, Y. Sheng, D.T. Nguyen, M. Wohlgenannt, A. Köhler, M.K. Al-Suti, M.S. Khan, Phys. Rev. B **72**(20), 205202 (2005)

[42] S. Schaefer, S. Saremi, K. Fostiropoulos, J. Behrends, K. Lips, W. Harneit, phys. stat. sol. (b) **245**(10), 2120 (2008)

[43] J. Behrends, A. Schnegg, K. Lips, E.A. Thomsen, A.K. Pandey, I.D.W. Samuel, D.J. Keeble, Phys. Rev. Lett. **105**(17), 176601 (2010)

[44] S.T. Hoffmann, F. Jaiser, A. Hayer, H. Bässler, T. Unger, S. Athanasopoulos, D. Neher, A. Köhler, J. Am. Chem. Soc. **135**(5), 1772 (2013)